EAI Endorsed Transactions
on Energy Web
Research Article EAI.EU

On-Site Protection Scheme for Microgrid with High Penetration Rate of Grid-Forming Inverter Interfaced Distributed Energy Resources

Yubo Yuan[1], Juan Li[1,*], Yunlong Jiang[1], Sudi Xu[1] and Haiou Cao[2]

[1]State Grid Jiangsu Electric Power Co. Ltd., Research Institute State, Nanjing 211103, China
[2]State Grid Jiangsu Electric Power Co. Ltd. Nanjing 210024, China

Abstract

INTRODUCTION: Renewable energy represented by grid forming inverter interfaced distributed energy resources is increasingly connected to microgrids that can operate independently and have various modes, resulting in traditional relay protection schemes that cannot meet the requirements of protection selectivity and speed.
OBJECTIVES: To this end, the fault characteristics of the grid forming distributed energy resources are analyzed. On this basis, the current, voltage and phase angle characteristics between them under the grid-connected/islanded operation mode of the microgrids are analyzed.
METHODS: Aiming at the problem that the traditional protection loses selectivity, the phase angle difference between the pre-fault voltage and the post-fault current is used to judge the fault direction, and the internal fault acceleration factor of the integrated phase angle difference and the measured impedance is used to improve the action equation of the inverse time overcurrent protection. Aiming at the problem that the fault current is too small and the inverse-time overcurrent protection cannot be started when the two-phase short-circuit fault occurs in the islanded state, a low-voltage protection criterion based on the comprehensive phase angle difference characteristics is set up, and a microgrid protection scheme combining improved inverse-time over-current protection and low-voltage protection is obtained.
RESULTS: The model is built by PSCAD, the theoretical analysis and simulation results show that the scheme can operate quickly and reliably in the grid-connected/islanded operation state of the microgrid.
CONCLUSION: The results verify the effectiveness of the proposed protection scheme.

Keywords: Microgrid, Inverter Interfaced Distributed Energy Resources, Voltage and Current Phase Angle Difference, Inverse-time Overcurrent Protection, Low Voltage Protection, Speed

Received on 18 February, accepted on 18 July 2025, published on 26 September 2025

doi: 10.4108/ew.10407

1. Introduction

In recent years, with the construction of modern energy systems, an increasing number of distributed energy resources (DERs) have been integrated into power systems [1-2]. Microgrids, which are composed of distributed generation units, distributed energy storage devices, and monitoring and protection devices, can operate safely and efficiently in local distribution networks and can also operate in islanded mode in small-scale distribution networks [3-4]. They are favored for their advantages of flexible operation and rapid response. The 14th Five-Year Plan for Modern Energy Systems proposes

*Corresponding author. Email: microgrid2025@163.com

to actively develop smart microgrids primarily aimed at absorbing new energy to achieve compatibility and complementarity with the main grid, and to encourage eligible key users to develop distributed energy resources and microgrids [5]. The synchronous development of the main grid and microgrids has been included in energy planning, outlining a new scenario for the future operation of China's power grid at the institutional level. However, microgrids with high penetration rates of inverter-interfaced distributed energy resources (IIDERs) exhibit significant differences in fault currents between grid-connected and islanded operation modes [6-7], and the direction of current is uncertain, posing challenges to the speed and selectivity of protection actions in microgrids [8-10].

1.1 Communication-Based Microgrid Protection Schemes

For example, Reference [10] studies the current phase response characteristics of IIDERs during low-voltage ride-through, proposes a fault direction identification method based on phase comparison of three sets of positive-sequence currents by analyzing the phase relationship between bus voltage and current fault components, and achieves fault section localization in microgrids through information transmission between unit protection modules. Reference [11] analyzes the fault current variations of IIDERs with low-voltage ride-through capability under different voltage sag levels, deeply discusses the influence law of different fault locations within the microgrid system on the current characteristics of each branch at the same bus, and proposes a fault direction determination method based on the phase difference comparison between the positive-sequence voltage fault component of the bus and the positive-sequence current fault components of each branch. Reference [12] regionalizes the microgrid, realizes real-time interaction of directional overcurrent information between adjacent protection devices through the Generic Object Oriented Substation Event (GOOSE) communication protocol, and achieves precise fault localization and isolation under complex microgrid operating conditions by leveraging the fast transmission characteristics of GOOSE tripping commands, adapting to challenges such as multiple power sources, multiple operation modes, and topological changes. Reference [13] proposes an ultra-high-speed traveling wave protection scheme based on detecting and analyzing traveling waves during microgrid faults, using the propagation characteristics of traveling waves in transmission lines to quickly locate and clear faults at extremely high speeds. Reference [14] divides microgrid protection areas into central layer, regional layer, and system layer according to fault impact diffusion, calculates protection action time using communication between layers and the inverse-time characteristics of differential current, and proposes an improved phasor calculation algorithm for inverse-time differential current protection. References [15, 16] determine faults through voltage and power change quantities respectively based on fault current phase relationships, both relying on communication at both ends of the bus. The schemes proposed in References [10-16] are applicable to both grid-connected and islanded operation modes of microgrids, but their implementation relies on communication systems, resulting in high requirements and costs for communication infrastructure.

1.2 Research on On-Site Microgrid Protection

In the field of on-site microgrid protection, Reference [17] uses programmable microprocessor-based directional element relays to set relays for different scenarios and installation locations, ensuring reliable operation in both grid-connected and islanded modes. However, this scheme has long protection action time and complex configuration, making it suitable as a backup protection. Reference [18] proposes a microgrid protection scheme based on frequency and voltage data processing, using voltage and frequency data as the action quantities for fault detection and corresponding relay tripping. Reference [19] improves existing sequence-domain directional elements by analyzing protection elements in the phase domain and sequence domain, and effectively uses them to accurately determine fault directions. However, in microgrids with high-proportion IIDERs, References [18, 19] may face increased difficulty in fault detection due to the complexity and uncertainty of fault currents. For situations where the Point of Common Coupling (PCC) is located on a feeder, existing studies consider hybrid microgrid schemes involving fault currents and voltages. Reference [20] proposes an alternating protection scheme for multiple microgrids in grid-connected and islanded operation modes based on current and voltage line parameters, considering fault conditions in multi-microgrids, which can be used for asymmetric fault detection in multi-microgrids with high renewable energy penetration. References [21, 22] improve the action speed of protection by modifying inverse-time overcurrent protection, applicable to both grid-connected and islanded states, but the schemes only consider single-sided protection on microgrid tie feeders and do not address how inverse-time overcurrent protection initiates when fault currents are small in microgrids. Reference [23] proposes collecting current and voltage signals to calculate complex power and precisely locate microgrid faults by comparing changes in complex power (including active and reactive power), but the scheme has a large computational load, imposing high requirements on system real-time performance and computing capabilities. Additionally, schemes using non-power-frequency signal injection[24], controller harmonic analysis[25], bifurcation theory[26], short-time correlation transformation[27], etc., to achieve microgrid protection are complex to implement and may increase costs. These new protection schemes for microgrids with high-proportion IIDERs significantly alter

traditional protection frameworks while increasing the implementation costs of the protection schemes.

In summary, current research on on-site microgrid protection remains incomplete. There is an urgent need for an on-site protection scheme adaptable to both grid-connected and islanded operation modes. To address this, this paper proposes an integrated on-site protection method combining improved inverse-time overcurrent protection and low-voltage protection. This method identifies fault directions using the phase angle difference between pre-fault voltage and fault current, enabling selective and rapid local fault clearance in both operation modes without relying on communication, thus offering high economic efficiency.

2. Fault Characteristics of Grid-Forming IIDERs

According to the operation of IIDER in AC microgrids, converter-interfaced generators are roughly divided into three types [22-24]: grid-following (GFL), grid-forming (GFM), and network-supporting. Most existing literatures mainly analyze GFL-type IIDER, which adjusts the converter output by measuring the phase information of the point of common coupling (PCC) through a phase-locked loop. However, this type may have stability issues in microgrids with weak system strength and low physical inertia. GFM-type IIDER possesses capabilities similar to synchronous machines, capable of autonomously maintaining the stability of power angle, frequency, voltage, etc., and can provide support for the system in microgrids with high-proportion IIDER. As the proportion of IIDER in microgrids increases, GFM-type IIDER will inevitably occupy a more important position in future microgrids [25-26]. This section analyzes GFM-type IIDER as the basis for subsequent analysis of fault characteristics in microgrids with high-proportion GFM-type IIDER.

Grid-forming IIDERs have the attribute of voltage sources, and the current level they can provide during faults is limited by the overcurrent of power electronic switches. The equivalent models of grid-forming IIDERs are a controlled current source (C-CS) or a controlled voltage source (C-VS). During a short circuit, grid-forming IIDERs react instantaneously (with a drop in $\dot{U}_t$). When $I_k < I_{max}$, they are modeled as C-VS; when $I_k \geq I_{max}$, they are modeled as C-CS, as shown in Equations (1) and (2):

$$\dot{I}_k = \frac{(\dot{U}_k - \dot{U}_t)}{Z_k} \quad , \quad |\dot{I}_k| < I_{max} \tag{1}$$

$$|\dot{I}_k| = I_{max} \quad , \quad |\dot{I}_k| \geq I_{max} \tag{2}$$

where $\dot{U}_k$ and $\dot{I}_k$ are the internal output voltage and current of the inverter, Z_k is the internal equivalent impedance of the inverter, $\dot{U}_t$ is the voltage at the point of common coupling (PCC) of the distributed energy resource, and I_{max} is the maximum output current of the distributed energy resource. In power system short-circuit calculations, grid-forming IIDERs are modeled as current sources with Z_k being infinitely large (open circuit).

Grid-forming IIDERs must possess robust fault ride-through capabilities. GB/T 29319—2024 Technical Specifications for Connecting Photovoltaic Power Generation Systems to Distribution Networks [27] includes requirements for the low-voltage ride-through of IIDERs. Define the voltage sag coefficient $\partial = U_t / U_N$, where U_N is the rated system voltage. When I_{max} is set to 1.2 p.u., the entire fault ride-through process and fault characteristics of grid-forming IIDERs [28] are presented in Table 1.

Table 1. Fault Ride-Through Process and Characteristics of Grid-Forming IIDERs

Voltage Sag Coefficient / ∂	Current amplitude /p.u.	current phase angle / o	grid disconnection time /s	Current Limitation Mode
0.5215-0.9	1.12-1.2	0-17	1.26~2	C-VS
0.4333~0.5215	1.2	17~90	1.08~1.26	C-CS
0.2~0.4333	1.2	90	0.625~1.08	constant current source
0~0.2	1.2	90	0~0.625	constant current source

3. Fault Characteristic Analysis of Microgrid

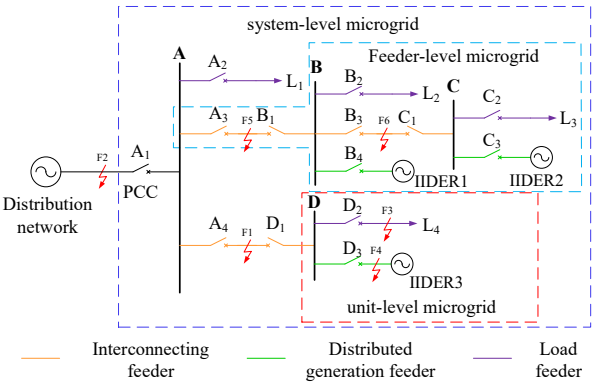

Figure 1. Microgrid Model

Microgrids are classified by scale into system-level microgrids, feeder-level microgrids, and unit-level microgrids [29-31]. Flexible switching between different forms can be achieved as needed to improve the power supply reliability of microgrids. In the microgrid shown in Fig. 1, a feeder with one end connected to a busbar and the other end directly connected to a load or IIDER is denoted as a branch feeder (including load feeders such as L_1 and distributed energy resource feeders such as IIDER1), while a feeder with both ends connected to busbars is denoted as a tie feeder, such as B_3C_1. In the analysis of fault characteristics, taking the unit-level microgrid powered by busbar D in Fig. 1 (hereinafter referred to as the D-unit microgrid) as an example, the phase angle difference characteristics between pre-fault voltage and fault current at the protection locations are analyzed for three scenarios: the grid-connected operation state of the D-unit microgrid, the independent operation state of the D-unit microgrid, and the islanded operation state of the D-unit microgrid within the system-level microgrid (non-independent operation state). Additionally, the current and voltage characteristics during two-phase short circuits in islanded states with potentially small short-circuit currents are analyzed.

3.1 Fault Characteristics in Grid-Connected State

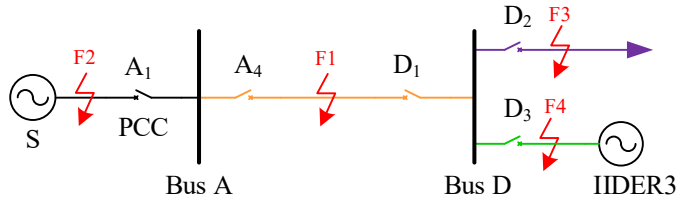

Figure 2. Simplified model of grid-connected D unit microgrid

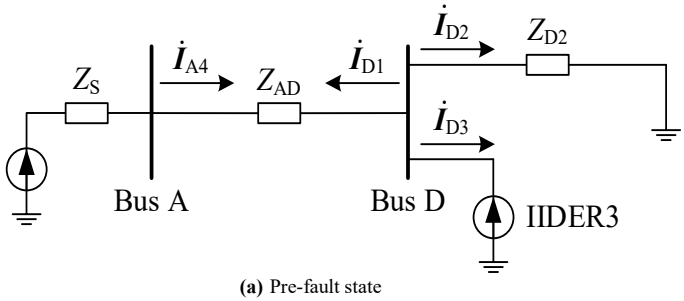

(a) Pre-fault state

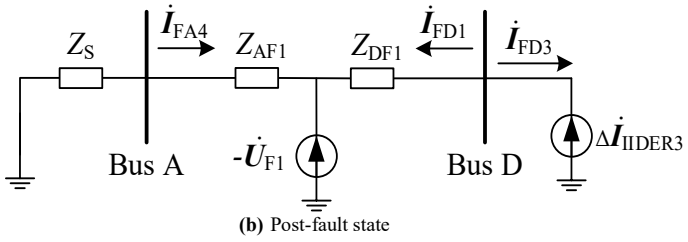

(b) Post-fault state

Figure 3. Grid-connected D unit microgrid F1 fault quivalent network

For ease of understanding, the analysis model of the microgrid is simplified. Take the distribution network and unit-level microgrid connected on both sides of the A_4D_1 busbar as an example, as shown in Fig. 2. Assuming a fault occurs at point F1 on the tie feeder, the fault network can be equivalent to the superposition of the non-fault state of the system before the fault and the fault (fault additional state), as shown in Fig. 3.

The current reference direction is defined as pointing from the busbar to the protected line. Before the fault, the current flowing through protection A_4 and protection D_1 are given by:

$$\dot{I}_{A4} = -\dot{I}_{D1} = \frac{\dot{U}_A - \dot{U}_D}{Z_{AD}} \tag{3}$$

The fault components of the current at protection A_4 and protection D_1 are given by:

$$\dot{I}_{FA4} = \frac{-(-\dot{U}_{F1})}{Z_S + Z_{AF1}} = \frac{\dot{U}_{F1}}{Z_S + Z_{AF1}} \tag{4}$$

$$\dot{I}_{FD1} = -\dot{I}_{FD3} = -(-\Delta\dot{I}_{IIDER3}) = \Delta\dot{I}_{IIDER3} \tag{5}$$

When a fault occurs at point F1, the currents at protection A4 and protection D1 are respectively:

$$\dot{I}'_{A4} = \frac{\dot{U}_A - \dot{U}_D}{Z_{AD}} + \frac{\dot{U}_F}{Z_S + Z_{AF1}} \tag{6}$$

$$\dot{I}'_{D1} = -\frac{\dot{U}_A - \dot{U}_D}{Z_{AD}} + \Delta\dot{I}_{IIDER3} \tag{7}$$

It is assumed that the system impedance angle is the same as the line impedance angle, and the line resistance is ignored. The corresponding voltage and current phasor relationships are shown in Fig. 4.

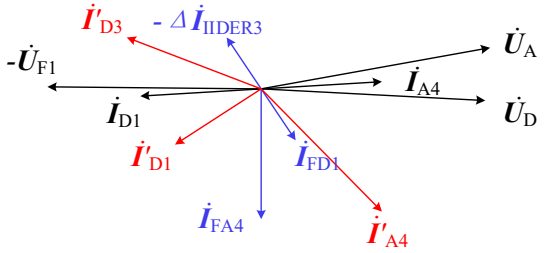

Figure 4. Grid-connected D unit microgrid F1 fault phase angle diagram

From Figure 4, it can be observed that:

Both $\dot{I}'_{A4}$ and $\dot{I}'_{D1}$ lag behind the pre-fault voltage, while $\dot{I}'_{D3}$ leads the pre-fault voltage.

For protection A4, the phase angle difference between $\dot{U}_A$ and $\dot{I}'_{A4}$ is $\Delta\phi_{A4} = \arg(\dot{U}_A / \dot{I}'_{A4}) > 0°$, indicating a positive phase angle difference between the pre-fault voltage and fault current.

For protection D1, the phase angle difference between $\dot{U}_D$ and $\dot{I}'_{D1}$ is $\Delta\phi_{D1} = \arg(\dot{U}_D / \dot{I}'_{D1}) > 0°$, also indicating a positive phase angle difference.

For protection D3, the phase angle difference between $\dot{U}_D$ and $\dot{I}'_{D3}$ is $\Delta\phi_{D3} = \arg(\dot{U}_D / \dot{I}'_{D3}) < 0°$, indicating a negative phase angle difference.

Analyzing the fault characteristics when faults occur at F2 (distribution network side), F3 (load feeder), and F4 (distributed power feeder) in the grid-connected microgrid, it is found that for positive-direction faults under grid-connected operation, the phase angle difference between the pre-fault positive-sequence bus voltage and the post-fault positive-sequence fault current at the protection location all falls within the range of $(0°, 180°)$.

3.2 Fault Characteristics in Islanded State

A unit-level microgrid is the smallest power supply unit in a microgrid with independent operation capability. When it operates independently, the tie feeder A_4D_1 is disconnected, and the D unit microgrid is in a source-load balance state. If a fault occurs at point F3 on the load feeder, the fault network can be equivalent to the superposition of the non-fault state of the system before the fault and the fault additional state, as shown in Figure 5.

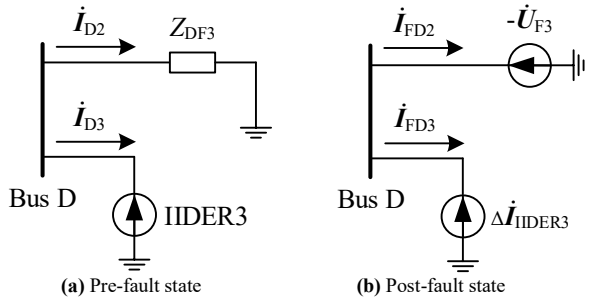

Figure 5. Stand-alone D unit microgrid F3 fault equivalent

The currents flowing through protections D_2 and D_3 before the fault are:

$$\dot{I}_{D2} = -\dot{I}_{D3} = \dot{I}_{IIDER3} \quad (8)$$

The fault components of the current at protection D_2 and protection D_3 are given by:

$$\dot{I}_{FD2} = -\dot{I}_{FD3} = \Delta\dot{I}_{IIDER3} \quad (9)$$

When a fault occurs at point F3, the currents at protections D_2 and D_3 are given by equation (10).

$$\dot{I}'_{D2} = -\dot{I}'_{D3} = \dot{I}_{IIDER3} + \Delta\dot{I}_{IIDER3} \quad (10)$$

The corresponding voltage and current phasor relationships are shown in Figure 6.

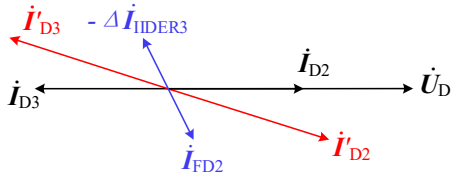

Figure 6. Stand-alone D unit microgrid F3 fault phase angle diagram

As can be seen from Figure 6: $\dot{I}'_{D2}$ lags behind the pre-fault voltage, while $\dot{I}'_{D3}$ leads the pre-fault voltage. It can be concluded that:

For protection D_2, the phase angle difference between $\dot{U}_D$ and $\dot{I}'_{D2}$ is $\Delta\phi_{D2} = \arg(\dot{U}_D / \dot{I}'_{D2}) > 0°$, indicating a positive phase angle difference between the pre-fault voltage and the fault current;

For protection D_3, the phase angle difference between $\dot{U}_D$ and $\dot{I}'_{D3}$ is $\Delta\phi_{D3} = \arg(\dot{U}_D / \dot{I}'_{D3}) < 0°$, indicating a negative phase angle difference between the pre-fault voltage and the fault current.

Similarly, analyzing the fault characteristics when faults occur in the load feeder, distributed power feeder, and tie feeder of the non-standalone microgrid, it can be seen that when a fault occurs in the positive direction of the protection in the islanded state, the phase angle difference between the pre-fault bus positive-sequence voltage and the post-fault positive-sequence fault current at the protection location also falls within the range of $(0°, 180°)$.

3.3 Analysis of Current and Voltage Characteristics During Two-Phase Short Circuit in Islanded State

When a two-phase short circuit occurs on the tie feeder of an islanded microgrid, the fault current is much smaller than that in other fault conditions, which may cause the inverse-time overcurrent protection to fail to start normally. Therefore, the fault characteristics during a two-phase short circuit are analyzed. Taking the fault at point F6 in

Figure 1 as an example (the equivalent circuit is shown in Figure 7), the power supply object of IIDER2 is the parallel connection of positive-sequence and negative-sequence load impedances.

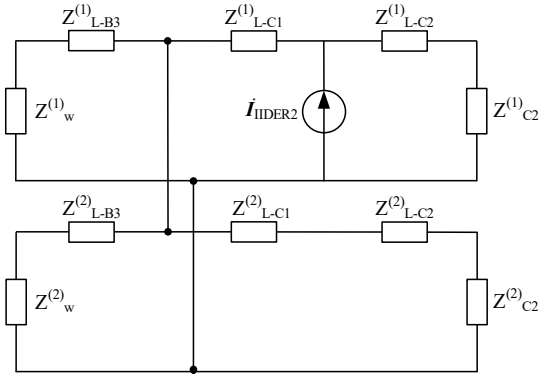

Figure 7. F6 two-phase short-circuit fault system side switch after tripping equivalent circuit

1. In Figure 7, Z_W is the equivalent impedance on the left side of the fault point. After the parallel connection of impedances on the left side, Z_W decreases further, so the shunt current on the left side of the fault point cannot be ignored. Analysis from Figure 7 shows that:

If there are many parallel lines on the left side of the fault point, the total impedance on the left side will be slightly smaller than that on the right side. The specific currents flowing through protections C_1 and C_2 need to be calculated based on impedance current division. Meanwhile, the increase in measured impedance will also prolong the action time of the inverse-time overcurrent protection.

2. The maximum fault current flowing through the load branch is 1/2 of the fault current output by the distributed power source. Since the penetration rate of this unit microgrid is 100%, the fault current output by the distributed power source is 1.2 times the rated current. Therefore, the fault current during a two-phase short circuit may be lower than the current during normal operation, making it impossible to detect the fault based on the current value.

3. The voltage across C_1 is no more than 50% of the normal voltage, and the voltage at all protections in the entire system drops. Due to the small short-circuit current and the short length of the lines in the microgrid, the voltage differences at each protection installation location are not significant.

3.4 Summary

Based on the above analysis, it can be concluded that:

1. In various scenarios, the phase angle difference between the pre-fault bus positive-sequence voltage and the post-fault positive-sequence fault current falls within the range of $(0°, 180°)$. Therefore, the phase angle characteristics between the pre-fault positive-sequence voltage of the bus and the positive-sequence fault current of each feeder can be used to reliably distinguish between forward and reverse faults.

2. For the problem that the fault current is too small to start the current protection during two-phase short circuit in the islanded state, the characteristics of phase angle difference and voltage drop during the fault can be comprehensively used to achieve fault clearance.

4. Microgrid Protection Scheme

In microgrids with a high proportion of IIDER (interfaced inverter-based distributed energy resources), the magnitude and direction of fault currents differ from those in traditional distribution networks. Inverse-time overcurrent protection has garnered attention from scholars in microgrid protection research due to its ability to determine fault interruption time based on the magnitude of short-circuit currents. However, in microgrids with high penetration of grid-forming IIDER, the short-circuit currents are relatively small, which may cause traditional inverse-time overcurrent protection to refuse operation due to failing to reach the starting current threshold. Meanwhile, the bidirectional nature of current flow in microgrids may lead to misoperation of traditional inverse-time overcurrent protection. Additionally, relying solely on voltage quantities is often insufficient to meet the selectivity requirements of protection. Therefore, Through analyzing the fault characteristics of microgrids in grid-connected and islanded operation modes, this paper proposes a microgrid protection method that comprehensively utilizes voltage and current characteristics before and after faults. This method achieves fast and selective fault removal in both grid-connected and islanded microgrid modes. Relying solely on local information without requiring communication equipment, it offers good economic performance. The specific formulation of the protection action equations and the setting process are described as follows.

4.1 Protection Action Equations

Improved Inverse-Time Overcurrent Protection

By introducing the phase angle difference between the proposed pre-fault positive-sequence voltage and post-fault positive-sequence current, as well as the measured impedance, into the inverse-time overcurrent protection action equation, an inverse-time overcurrent protection action equation suitable for microgrid protection can be obtained, as shown in Equation (15)

$$t = \frac{0.14 \cdot t_{\mathrm{TDS}m.ij} \cdot M'}{(I_{\mathrm{f}} / I_{\mathrm{op}m.ij}) - 1} \tag{15}$$

Where: M' denotes the internal fault acceleration factor integrating the phase angle difference and measured impedance, with $M' = (\sin\alpha_{ij} / |\sin\alpha_{ij}|) \cdot (Z_m / Z_{line})$. $t_{TDSm.ij}$ is the time setting coefficient for protection *ij* in grid-connected/islanded modes. *i* is the bus number (e.g., A, B, C, D in Figure 1), and *j* is the feeder number (e.g., 1, 2, 3, 4 in Figure 1).*m* represents the microgrid operation state, where G denotes grid-connected and I denotes islanded. I_f is the fault current value. $I_{opm.ij}$ is the starting current of protection *ij*. $\alpha_{ij} = \arg(\dot{U}_i / \dot{I}'_{ij})$ is the phase angle difference between the pre-fault voltage and post-fault current. $\dot{U}_i$ is the pre-fault voltage at bus i, and $\dot{I}'_{ij}$ is the post-fault current flowing through feeder *ij*. Z_m is the measured impedance (the measured voltage uses the pre-fault memory voltage). Z_{line} is the line impedance from the protection installation point to the end of the feeder.

It can be seen from Equation (15) that the improved inverse-time overcurrent protection action equation includes the following elements:

1. When the microgrid is operating in grid-connected mode, the system-side power supply and distributed power sources jointly provide short-circuit current, which can reach 6 to 8 times the rated current. When the microgrid is in islanded operation, the short-circuit current provided by distributed power sources can only reach 1.2 to 2 times the rated current. Therefore, the setting values of $I_{opG.ij}$ and $t_{TDSI.ij}$ under grid-connected state, and those of $I_{opI.ij}$ and $t_{TDSI.ij}$.

2. The role of M' : 1) It can be used to distinguish between forward and reverse faults. When forward fault current flows, ($(\sin\alpha_{ij} / |\sin\alpha_{ij}|) > 0$ and $t > 0$; when reverse fault current flows, ($(\sin\alpha_{ij} / |\sin\alpha_{ij}|) < 0$ and $t < 0$. 2) It can accelerate fault clearance. For nearby fault points, the measured impedance is used to accelerate fault removal. When the fault is inside the protection zone, $Z_m / Z_{line} < 1$, shortening the protection action time; when the fault is outside the protection zone, $Z_m / Z_{line} > 1$, prolonging the protection action time.

Low Voltage Protection

According to GB/T 14285-2023 Technical Regulations for Relay Protection and Safety Automatic Devices and GB/T 29319-2024 Technical Specifications for Photovoltaic Power Generation Systems Connected to Distribution Networks, when the voltage is lower than 85% of the rated voltage (U_N), it is considered an abnormal operating state, and the distributed power source is in a low-voltage ride-through state. The faulty line should be quickly cut off to restore power supply to the non-fault area. Combining voltage protection with angle criteria, the low-voltage action threshold is set based on the abnormal voltage operating state. When the line voltage drops below 85% U_N and the angle criterion confirms a forward-direction fault, the protection action criterion is jointly composed of low-voltage protection and angle criterion. The action conditions for low-voltage protection are:

$$\begin{cases} U_{opm.ij} < 0.85\text{p.u.} \\ (\sin\alpha_{ij} / |\sin\alpha_{ij}|) > 0 \end{cases} \tag{16}$$

4.2 Protection Parameter Setting

In order to ensure coordination between upper and lower level protections, appropriate protection parameters must be selected according to the different locations of protections. Taking the microgrid shown in Figure 1 as an example, the setting is carried out for three types of feeders: distributed generation feeders, load feeders, and tie feeders. The setting process of protection parameters is illustrated by taking the tie feeder as an example.

1. Improved Inverse-Time Overcurrent Protection in Grid-Connected State

1) Pickup current value

First, calculate the starting current values at the installation locations of each protection near the system side in the grid-connected state. Taking the line D_1-A_4-A_3-B_1-B_3-C_1 in Figure 1 as an example, to ensure the selective operation of protections A_4、A_3 and B_3 near the system side, the curve shape coefficients and translation coefficients of the action equations of each protection are consistent. The starting current parameters can be set according to Equation (17):

$$I_{opG.ij} = K_{rel} K_{ss} / K_{re} \cdot I_{ij.max} \tag{17}$$

For the protections D_1、B_1、C_1 far from the system side, the detected current during normal operation is mainly load current. When a fault occurs on the tie feeder, the current flowing through is primarily the reverse fault current provided by distributed power sources. According to the power supply characteristics of the microgrid, IIDERs (inverter-interfaced distributed energy resources) near the end of the line and close to users should supply power locally, with surplus power fed into the main grid. In microgrid planning and design, the balance between new energy output and load power must be considered. The setting of protection parameters for the protections far from the system side should be divided into two cases according to the source-load ratio λ of the microgrid units they carry, and the setting formulas are:

$$I_{opG.ij} = \begin{cases} (1.1\lambda - 0.5) I_L & \lambda \geq 0.455 \\ 0 & \lambda < 0.455 \end{cases} \tag{23}$$

2) Time setting coefficient

To ensure the time coordination of protections, protection B_3 is first set. The starting current of B_3 is denoted as $I_{opG.B3}$. According to the selectivity

requirement, when the most severe fault occurs at the outlet of line C_2, the operating time of protection B_3 should be Δt higher than that of protection C_2. Since protection C_2 operates instantaneously, the operating time of protection B_3 can be set as $t_{B3} = \Delta t$. Substituting this into Equation (15), the time constant of protection B_3 can be obtained, as shown in Equation (24):

$$t_{TDSG.B3} = \frac{[(I_{f.C2.max} / I_{opG.B3}) - 1]\Delta t}{0.14 \cdot M'} \quad (24)$$

For protection A_3, when the most severe fault occurs at the outlet of line B_3C_1 (near B_3), the operating time of protection A_3 should be Δt higher than that of protection B_3. The setting process is similar to that of protection B_3.

2. Low Voltage Protection

1) Pickup voltage value

$$U_{opm.ij} = 0.85 \text{p.u.} \quad (26)$$

2) Time setting coefficient

According to the setting of the action time for the improved inverse-time overcurrent protection in the previous text, the three-phase short circuit can be cleared within 0-0.2s. Setting the fastest action time of the low-voltage protection as 0.2s, and then sequentially setting the action times of the cooperating protections in a stepwise manner can maximize the selectivity of the low-voltage protection action.

5. Case Study and Simulation Verification

In PSCAD, a microgrid simulation model with IIDER as shown in Figure 1 is built. The voltage level of the microgrid is 10kV, the frequency is 50Hz, and it is connected to the main grid through a 10kV/110kV step-up transformer. Distributed power sources all adopt PQ control strategies with low-voltage ride-through capability, among which the capacity of IIDER1-IIDER3 is 3MW each, and the maximum fault current is 1.2 times the rated current. The length of each tie feeder is 2km, the length of each load feeder is 0.2km, and the length of each distributed power feeder is 0.1km. The line impedance is lZ=(0.125+j0.405)Ω/km. The capacity of each load is 3MV·A, and the power factor is 0.85. Let Δt=0.2s, t_b=0.04s. When the microgrid transitions from grid-connected operation to islanded operation, the PCC point (A_1) and the load L1 are disconnected. The fault points on the tie feeder are set at 1800m from the protection A_3, A_4, B_3 line and 1800m from the protection B_1, C_1, D_1 line respectively.

According to the microgrid protection setting scheme described in this document, the protection for the microgrid in grid-connected and islanded states is set. PSCAD is used to build the protection action logic module of the microgrid, set the starting current and time constants, and simulate the protection of the entire system. Different types of faults are set at different fault points, and the original data collected by each circuit breaker and the actual action conditions are recorded.

1. Grid-connected state

Different types of faults are set on the tie feeder, and the action conditions of each protection obtained through simulation are shown in Table 2.

Table 2. Protective action of the contact feeder for faults at a distance of 1800m from the protective installation under grid-connected state

Protection Location	Fault current /kA	Fault Voltage /kV	Angle α_{ij} / °	Fault Type	Action Time/s
C1	0.203	0.185	-255.320	three	0.228
	0.194	3.042	-230.279	two	0.700*
B3	2.677	2.228	72.485	three	0.208
	1.320	4.073	67.535	two	0.300*
B1	0.393	0.363	-252.302	three	0.193
	0.387	3.100	-227.773	two	0.500*
A3	4.228	3.614	75.664	three	0.213
	2.008	4.723	69.494	two	0.500*
A4	5.687	2.918	-281.990	three	0.227
	2.807	4.365	75.496	two	0.300*
D1	0.204	0.133	-251.670	three	0.229
	0.201	2.983	-226.071	two	0.700*

Note: The action time marked with * in Tables 2 and 3 indicates tripping by low-voltage protection, the"three" indicates three-phase short circuit, and the "two" indicates two-phase short circuit

In Table 2, the action conditions of each protection are recorded when three-phase short circuit or two-phase short circuit faults occur at 1800m from the protection installation location on the tie feeder in the grid-connected state of the microgrid. When a three-phase short circuit occurs, the protection action time of the tie feeder is less than 0.01s, and the action time of the three-phase short circuit at 1800m from the protection installation location on the tie feeder is approximately 0.2s. When a two-phase short circuit fault occurs, the protection action time on the tie feeder is still less than 0.01s, and the action time on the tie feeder is the tripping time of the low-voltage protection, indicating that the action time of the low-voltage protection is faster at this time. Simulation of the grid-connected microgrid system configured with only improved inverse-time overcurrent protection shows that the action times of protections B3, B1, A3, and A4 are less than 2s during two-phase short circuit. Although the short-circuit current is small at this time, the improved inverse-time overcurrent protection can still act within 2s. However, the action times of protections C1 and D1 are as long as 4-6s, which is because the short-circuit current provided by distributed power sources is small, and the load impedance and other branch impedances in the measured impedance are large, leading to a further increase in action time.

2. In the islanded state (with the PCC point disconnected)

Different types of faults are set on the tie feeder, and the action conditions of each protection obtained through simulation are shown in Table 3.

Table 3. Protective action of the contact feeder for faults at a distance of 1800m from the protective installation under islanded state

Protection Location	Fault current /kA	Fault Voltage /kV	Angle α_{ij} / °	Fault Type	Action Time/s
C1	0.204	0.174	-325.530	three	0.223
	0.099	3.451	-325.575	two	0.700*
B3	0.393	0.336	-324.214	three	0.233
	0.187	3.493	-324.184	two	0.300*
B1	0.396	0.338	-324.165	three	0.209
	0.188	3.492	-324.341	two	0.500*
A3	0.202	0.172	-324.988	three	0.216
	0.096	3.449	-324.957	two	0.500*
A4	0.385	0.198	-323.076	three	0.221
	0.181	3.427	-323.587	two	0.300*
D1	0.205	0.105	-325.904	three	0.209
	0.102	3.403	-325.946	two	0.700*

According to Table 3, when a three-phase short circuit occurs at 1800m from the protection installation location on the tie feeder, the protection action time is approximately 0.2s. When a two-phase short circuit occurs at this location, the fault is cleared by the voltage protection.

Simulation of the islanded microgrid system configured only with improved inverse-time current protection shows that the short-circuit current is small, failing to reach the current pickup value, or even if it can reach the pickup value, the inverse-time action time is as long as 20s. However, the circuit breaker can detect that the voltage is lower than 0.85p.u. and $(\sin\alpha_{ij} / |\sin\alpha_{ij}|) > 0$, triggering the low-voltage protection and acting after a certain delay.

From the above simulation results, it can be seen that the microgrid protection method proposed in this paper comprehensively utilizes fault characteristics such as voltage, current, and angle. In both grid-connected and off-grid states, the protections at various locations can operate correctly with good rapidity.

By introducing the phase angle difference to determine the fault direction and incorporating the measured impedance to accelerate the protection response for internal faults, the selectivity of the protection is ensured through the setting of time coordination relationships. By cooperating with low-voltage protection, the action time is guaranteed when the fault current is small or fails to reach the starting current value, ensuring the rapidity of the protection. Through the setting of the starting current and time coordination relationships, it is ensured that for any type of short-circuit fault at any fault location in the microgrid's grid-connected/off-grid modes, the circuit breaker will correctly operate with the smaller action time between the improved inverse-time overcurrent protection and the low-voltage protection, ensuring the sensitivity and reliability of the protection. This protection scheme meets the performance requirements of microgrid protection and relies on local information without the need for communication equipment, offering good economic efficiency.

6. Conclusions

This paper proposes a grid-connected/off-grid protection method for microgrids with high-proportion grid-forming IIDERs (Inverter Interfaced Distributed Energy Resources). The method uses the phase angle difference between the pre-fault voltage and post-fault current to determine the fault direction, accelerates the protection response for internal faults using measured impedance, and comprehensively utilizes voltage and current characteristics during faults to achieve fast and selective fault clearance in both grid-connected and off-grid modes of microgrids. The main conclusions are as follows:

1. By analyzing the voltage and current phase angles of each line in the microgrid under different fault locations in grid-connected/off-grid states using the fault equivalent network, it is concluded that the fault direction can be identified based on the phase angle difference between the pre-fault voltage and the fault current.

2. An internal fault acceleration factor that integrates the comprehensive phase angle difference and measured impedance is introduced into the inverse-time action equation, addressing the issues of traditional current protection in microgrids, such as misoperation and longer action times closer to the power source. A microgrid low-voltage protection scheme assisted by a phase angle difference criterion is proposed, overcoming the problem of action blind zones where current protection fails to activate during two-phase faults in off-grid states.

3. The parameter setting process and time coordination logic of the proposed protection scheme are thoroughly demonstrated. Through PSCAD/EMTDC simulations, it is verified that the proposed protection scheme can adapt to the grid-connected/off-grid operation modes of microgrids, meeting the requirements of rapidity, reliability, selectivity, and sensitivity. The implementation of the method relies on local information without the need for communication equipment, offering good economic efficiency.

In the criteria constructed in this paper, measured impedance is used to accelerate the protection action time for internal faults. The influence of transition resistance is not yet considered. In the follow-up research, the adaptability of the protection scheme under faults with transition resistance will be studied.

Acknowledgements.
This work was supported by the project supported by State Grid Jiangsu Electric Power Company Technology Project (J2023163).

References

[1] Zhiyuan G, Jing Z, Weijin Z, et al. Thoughts on some characteristics of the new power system[J]. Electric Power Automation Equipment, 2023, 43(6): 137-143+151.
[2] Kuizhong Z. Optimal Design of Photovoltaic-Storage-Charging Microgrid System for New Industrial and Commercial Parks under the Double Carbon Background[J]. Electrical Age, 2025, (01): 42-44.
[3] Bingyin X. Relay Protection Technology and Its Development in Modern Distribution Networks[J]. Distribution & Utilization, 2024, 41(08): 65-74+87.
[4] Changjie Y, Nan Q, Kai S, et al. Development Status and Prospect of Distributed Energy in China[J]. Distributed Energy, 2023, 7(02): 1-7.
[5] Chengshan W, Yue Z. Overview of Microgrid Demonstration Projects[J]. Distribution & Utilization, 2015, (01): 16-21.
[6] Daxing W, Yan N, Jingpei W, et al. Robust Simplified Modeling of Microgrids in the Context of Building a New Power System[J]. Electric Power, 2024, 57(1): 148-157.
[7] Min Z, Ying C, Chen S, et al. Characteristic Analysis and Demonstration Project Design of Microgrid Clusters[J]. Power System Technology, 2015, 39(06): 1469-1476.
[8] Jiale D. Research on Fault Analysis and Active Protection Methods for AC Microgrids[D]. Yangzhou: Yangzhou University, 2024.
[9] Ying W. Research on Fault Detection Methods and Protection Principles for Microgrids[D]. Hangzhou: Zhejiang University, 2017.
[10] Liuming J, Yibo W, Tong Z, et al. Protection Method for AC Microgrid Considering Low Voltage Ride-Through Characteristics of Photovoltaic[J]. Electric Power Automation Equipment, 2022, 42(05): 54-60.
[11] Haijuan H, Longhua M, Fan Z, et al. Microgrid Protection Considering Low Voltage Ride-Through of IIDG[J]. Proceedings of the CSEE, 2017, 37(1): 110-120.
[12] Shishuai Z, Yajun Z, Chenghong T, et al. Fault Location and Isolation in Microgrid Based on GOOSE Communication Technology[J]. Automation of Electric Power Systems, 2015, 39(12): 179-183.
[13] Saleh KA, Hooshyar A, El-Saadany EF. Ultra-High-Speed Traveling-Wave-Based Protection Scheme for Medium-Voltage DC Microgrids[J]. IEEE Transactions on Smart Grid, 2019, 10(2): 1440-1451.
[14] Wentao H, Nengling T, Jianqing L, et al. Multi-Layer Collaborative Inverse-Time Protection Scheme for Microgrids[J]. Transactions of China Electrotechnical Society, 2021, 36(03): 623-633.
[15] Shijin Z, Jin H, Fan Y, et al. Microgrid Protection Scheme Based on Improved Current Phase Difference Protection[J]. Electrical Measurement & Instrumentation, 2023, 60(09): 132-137.
[16] Wang B, Jing L. A Protection Method for Inverter-Based Microgrid Using Current-Only Polarity Comparison[J]. Journal of Modern Power Systems and Clean Energy, 2020, 8(03): 446-453.
[17] Fan L. Control and Dynamics in Power Systems and Microgrids[M]. London: Taylor and Francis CRC Press, 2017.
[18] Srivastava A, Parida S K. Frequency and Voltage Data Processing Based Feeder Protection in Medium Voltage Microgrid[C]. 2019 IEEE PES Innovative Smart Grid Technologies Europe (ISGT-Europe), 2019: 1-5.
[19] Lahiji H, Ajaei BF, Boudreau RE. Non-Pilot Protection of the Inverter-Dominated Microgrid[J]. IEEE Access, 2019, 7(1): 142190-142202.
[20] Altaf MW, Arif MT, Saha S, et al. Effective Protection Scheme for Reliable Operation of Multi-Microgrid[C]. 2020 IEEE International Conference on Power Electronics Drives and Energy Systems (PEDES), 2020: 1-6.
[21] Yongli L, Qiang J, Botong L, et al. Application of Inverse-Time Overcurrent Protection Based on Low Voltage Acceleration in Microgrid[J]. Journal of Tianjin University (Science and Technology), 2011, 44(11): 955-960.
[22] Cao Z, Ji L, Chang X, et al. Inverse-Time Current Protection Method of Microgrid Based on Composite Fault Compensation Factor[J]. Power System Protection and Control, 2020, 48(20): 133-140.
[23] Prince SK, Affijulla S, Panda G. Protection of DC Microgrids Based on Complex Power During Faults in On/Off-Grid Scenarios[J]. IEEE Transactions on Industry Applications, 2023, 59(1): 244-254.
[24] Chongkai F, Longhua M, Rui O, et al. Research on Control-Protection Coordination Based Injection Protection Scheme of Microgrid[J]. Proceedings of the CSEE, 2023, 43(09): 3389-3402.
[25] El SWT, Azzouz MA, Zeineldin HH, et al. A Harmonic Time-Current-Voltage Directional Relay for Optimal Protection Coordination of Inverter-Based Islanded Microgrids[J]. IEEE Transactions on Smart Grid, 2021, 12(3): 1904-1917.
[26] Ahmadi S, Sadeghkhani I, Shahgholian G, et al. Protection of LVDC Microgrids in Grid-Connected and Islanded Modes Using Bifurcation Theory[J]. IEEE Journal of Emerging and Selected Topics in Power Electronics, 2021, 9(3): 2597-2604.
[27] Allahdadi K, Sadeghkhani I, Fani B. Protection of Converter-Interfaced Microgrids Using Modified Short-Time Correlation Transform[J]. IEEE Systems Journal, 2020, 14(4): 5172-5175.